ADVANCES IN ATMOSPHERIC SCIENCES, VOL. 23, NO. 5, 2006, 775–783

Applications of Conditional Nonlinear Optimal Perturbation to the Study of the Stability and Sensitivity of the Jovian Atmosphere

JIANG Zhina*[1,2](姜智娜)

[1] *State Key Laboratory of Numerical Modeling for Atmospheric Sciences and Geophysical Fluid Dynamics, Institute of Atmospheric Physics, Chinese Academy of Sciences, Beijing* 100029

[2] *Graduate University of the Chinese Academy of Sciences, Beijing* 100039

(Received 16 September 2005; revised 23 February 2006)

ABSTRACT

A two-layer quasi-geostrophic model is used to study the stability and sensitivity of motions on small-scale vortices in Jupiter's atmosphere. Conditional nonlinear optimal perturbations (CNOPs) and linear singular vectors (LSVs) are both obtained numerically and compared in this paper. The results show that CNOPs can capture the nonlinear characteristics of motions in small-scale vortices in Jupiter's atmosphere and show great difference from LSVs under the condition that the initial constraint condition is large or the optimization time is not very short or both. Besides, in some basic states, local CNOPs are found. The pattern of LSV is more similar to local CNOP than global CNOP in some cases. The elementary application of the method of CNOP to the Jovian atmosphere helps us to explore the stability of various-scale motions of Jupiter's atmosphere and to compare the stability of motions in Jupiter's atmosphere and Earth's atmosphere further.

Key words: stability, sensitivity, conditional nonlinear optimal perturbation, singular vector

doi: 10.1007/s00376-006-0775-x

1. Introduction

The general circulation of the Jovian atmosphere is dominated by multiple zonal jets associated with banded structures of clouds (Ingersoll, 1990). This is a great difference from the Earth's atmosphere, which has only one midlatitude westerly jet in each hemisphere. The mechanism of maintaining this basic feature is not yet resolved. Another fantastic phenomena is the Great Red Spot (GRS) located on the southern hemisphere, which has persisted for more than 300 years since it was discovered by Cassini in 1665. Even some small-scale vortices can persist for about 60 days unless they interact with each other (MacLow and Ingersoll, 1986). The GRS is a large-scale anticyclone, which is the rule rather than the exception throughout the solar system. One may even find analogs of Jovian vortices in Earth's oceans and atmosphere, for example, the Gulf Stream rings and the blocking highs (Dowling, 1993). The difference among the phenomena is that in Earth's atmosphere such events generally cannot persist for such a long time. So, the question why some anticyclones, e.g., the GRS and white ovals in Jupiter's atmosphere, can persist for such a long time needs to be answered.

Ingersoll and Cuong (1981) simulated the stable and unstable vortices with a two-layer quasi-geostrophic model, and showed that when two stable vortices collided, they will merge after a short transient phase to form a larger stable vortex rather than the non-interaction. They suggested the long-lived Jovian vortices maintain themselves against dissipation by absorbing the smaller vortices generated by convection. The method of numerical simulation in the research of stability and sensitivity of the Jovian atmosphere has been popular through the history of this research (Marcus, 1988; Achterberg and Ingersoll, 1994; Williams, 1996).

One of the useful tools in stability and sensitivity analysis is the linear singular vectors (LSVs), which were first applied to the meteorological research field by Lorenz (1965). The linear approximation is valid

*E-mail: jzn@mail.iap.ac.cn

if the initial perturbation is sufficiently small and the time period is not too long. But the motions of the Earth's atmosphere and Jupiter's atmosphere are both dominated by complicated nonlinear systems. In Mu and Duan (2003) and Mu et al. (2003), the concept of conditional nonlinear optimal perturbations (CNOPs) is introduced, and these are the extension of the linear singular vector into the nonlinear domain. Conditional nonlinear optimal perturbations are initial perturbations whose nonlinear evolution obtains the maximum value of the objective function, which is constructed according to the physical problem that we are interested in, while the linear singular vectors are the initial perturbations that have the largest growth rate in the linear regime at the optimization time.

In this paper, we attempt to study the stability and sensitivity of motions on small-scale Jovian vortices with a two-layer quasi-geostrophic model by the method of conditional nonlinear optimal perturbations. Section 2 describes the model and the concept of CNOP. In section 3, CNOPs of three basic states are obtained. The characteristics of CNOP and the differences between CNOPs and LSVs are analyzed. Finally, section 4 gives the conclusions and the implications of the results.

2. The model and the CNOPs

Dowling and Ingersoll (1988) pointed out that two-layer models can simulate motions of vortices in Jupiter's atmosphere effectively. The upper-layer contains the vortices and all the time-dependent motions. The lower layer represents the neutrally stratified deep atmosphere. Any motions in the lower layer are assumed to be zonal and steady. The two-layer system can be reduced to a one-layer system with meridionally varying solid bottom topography (Gill, 1982).

We consider the following two-dimensional nondimensional quasi-geostrophic (QG) model for a single upper layer supported hydrostatically on a much deeper lower layer (Dowling and Ingersoll, 1988):

$$\begin{cases} \dfrac{\partial q}{\partial t} + J(\psi, q) = 0 \\ q = \nabla^2\psi - F\psi + f + F\psi_2 \quad \text{in } \Omega \times [0, T] \\ \psi|_{t=0} = \psi_0 \end{cases} . \tag{1}$$

The dependent variable is the upper layer streamfunction $\psi(x, y, t)$. The model differs from standard QG models only in the term $F\psi_2$, where $\psi_2(y)$ is the streamfunction of the zonal flow in the lower layer. q is the potential vorticity. F is the Planetary Froude number,

$$F = \left(\frac{L}{L_{\mathrm{R}}}\right)^2 = \frac{f_0^2 L^2}{gH_0(1 - \rho_1/\rho_2)} ,$$

where L_{R} is the Rossby deformation radius, L is the length scale, H_0 the typical characteristic height, f_0 Coriolis parameter, and ρ_1 and ρ_2 are the density of the upper and lower atmosphere respectively ($\rho_2 > \rho_1$). f is the nondimensional Coriolis parameter. $\Omega = [0, 2X] \times [0, 2Y]$ with a double periodic boundary condition.

Dimension analysis shows that $F\psi_2 \sim f$ (Dowling and Ingersoll, 1988). In this paper, for simplicity, the lower streamfunction $\psi_2(y)$ is defined as:

$$\psi_2(y) = \frac{f}{2F} \times \left[\sin\left(\frac{2\pi y}{2Y}\right) + 1\right] . \tag{2}$$

In our numerical approach, the five-point difference scheme is employed to discretize the Laplacian operator. The Arakawa finite difference scheme is used to discretize the Jacobian operator. The temporal discretization is carried out by using the Adamas-Bashforth scheme. The grid spacing is $\Delta x = 0.2$ and the time step is $\Delta t = 0.006$. $\Omega = [0, 6.4] \times [0, 3.2]$

For fixed $T > 0$ and initial condition $\psi|_{t=0} = \psi_0$, the propagator M is well-defined; $\psi(x, y, t) = M_T(\psi_0)$ is the solution of (1) at time T. The energy norm is employed in this paper,

$$\|\varphi\|^2 = \int_\Omega (|\nabla\varphi|^2 + F|\varphi|^2) dxdy , \tag{3}$$

where φ is the streamfunction.

In order to consider the influence of nonlinearity on predictability, Mu and Duan (2003) and Mu et al. (2003) proposed the concept of conditional nonlinear optimal perturbation (CNOP), which seeks an initial perturbation $\varphi_{0\sigma}^*$ that makes the objective function $J(\varphi_{0\sigma}^*)$ acquire a maximum value under the initial constraint condition $\|\varphi_0\| \leqslant \sigma$,

$$J(\varphi_{0\sigma}^*) = \max_{\|\varphi_0\| \leqslant \sigma} J(\varphi_0) , \tag{4}$$

where

$$J(\varphi_0) = \|M_T(\psi_0 + \varphi_0) - M_T(\psi_0)\| .$$

To calculate the conditional nonlinear optimal perturbation, the reciprocal of the objective function and its corresponding gradient with respect to the initial perturbation are determined. In this process, the variation method and adjoint technique are used. The deduction in detail can be found in the paper by Mu and Zhang (2006). Because of the large free degrees of the model, the optimization algorithm of the Spectral Projected Gradient (SPG) method is employed (Birgin et al., 2000), which calculates the least value of a function of several variables subject to box and ball constraints. In this paper, we just change the squared norm constraint into the energy norm constraint. Besides, this optimization method does not need to calculate the gradient of the norm of the initial perturbation with

respect to the initial perturbation itself, which is different from SQP (Powell, 1982) used in Mu and Zhang (2006). At present, the method of CNOP has been widely used in ocean and atmospheric research fields (Mu et al., 2003; Duan et al., 2004; Mu et al., 2004).

3. Numerical results

Williams and Yamagata (1984) pointed out that the primary arbitrary parameter in Jupiter's atmosphere is the Rossby deformation radius $L_{\rm R}$, and unless the atmosphere is both very deep and very stable, this value of $L_{\rm R} = 1500$ km is reasonable. Besides, the basic dimensional dynamical parameters for three distinct scales of vortices are given. For a small vortex, L=2000 km, U=10 m s^{-1}, and $f_0 = 2.5 \times 10^{-4}$ m s^{-2}. Dowling and Ingersoll (1988) observed that the layer thickness and the Coriolis parameter both vary substantially across the GRS, and they estimated that the QG approximation is good only to about the nearest 30%, while motions on the small scale observe the rule of the quasi-geostrophic approximation. So in this paper, the stability and sensitivity of motions in small-scale vortices with the QG model are studied.

In this section, two steady states and an unsteady state are taken as basic states to calculate CNOPs and LSVs for different initial constraint conditions. LSVs are obtained by maximizing a modified version of the objective function $J(\varphi_0)$, which is defined in the linear regime. The optimization algorithm employed is still the SPG method with the smallest constraint condition. Due to the linear characteristic of LSVs, multiplying an LSV by a constant yields another LSV.

3.1 *Experiment 1*

In this experiment, the initial basic state is chosen as

$$\psi_0(y) = a \times \sin\left(\frac{2\pi y}{2Y}\right) + b\,,$$

where $a = 4.62$ and $b = 44.643$. This is a steady state. According to Arnol'd's nonlinear stability criteria (Mu and Shepherd, 1994), this basic state is nonlinearly stable. The total energy norm of the basic state is 271.630. The maximum constraint condition σ of the initial perturbation is 2.72, which is approximately 1.0% of that of the basic state. There are 720 steps, which correspond to 10 days (on Earth), for the following experiments, and unless indicated otherwise, 10 days are always employed.

Table 1 summarizes the numerical results of Expt. 1. $\|\varphi_{\rm LL}\|$ and $\|\varphi_{\rm LN}\|$ represent the energy norms of the linear and nonlinear evolution of LSV with the prediction time. $\|\varphi_{\rm TL}\|$ and $\|\varphi_{\rm TN}\|$ are the energy norms of the linear and nonlinear evolution of CNOPs with the prediction time. $\lambda_{\rm L}$ is the singular value (SVa). For each σ, the corresponding LSV is obtained by multiplying the LSV with the smallest σ by a constant so that its energy norm is σ. CNOPs can be obtained by the nonlinear optimization method directly, and we find that they are all located on the boundary of the constraint. In particular, in some basic states, local CNOPs may also be found, which are located on the boundary too under the condition that the initial constraint condition σ is large. As for some σ values, if there is local CNOP, the upper cell in the table is the local CNOP and the nether cell is the global CNOP. From the table, one can see that when the initial constraint condition σ is very small, the norms of the linear and nonlinear evolutions of LSV and CNOP are almost the same, which proves that in the linear regime LSV can represent CNOP well. When the initial constraint condition becomes larger, LSV and CNOP show great differences gradually. Figure 1, which is plotted based on Table 1, also shows the value differences of energy norms between the linear and nonlinear evolution of LSV and CNOP respectively. Here, $\|\varphi'_{\rm TN}\|$ is the energy norm of the nonlinear evolution of the local CNOP with the prediction time.

Figure 2 shows LSV and CNOP and their corresponding linear and nonlinear evolutions under the small initial constraint condition σ=0.0272. The results show that whatever the patterns of CNOP and LSV or their corresponding linear and nonlinear evolutions are, they are almost the same. That is to say, under this condition, the linear approximation is valid. Figure 3 gives the local and global CNOP and their corresponding nonlinear evolutions respectively under the large initial constraint condition $\sigma = 1.0$. The re-

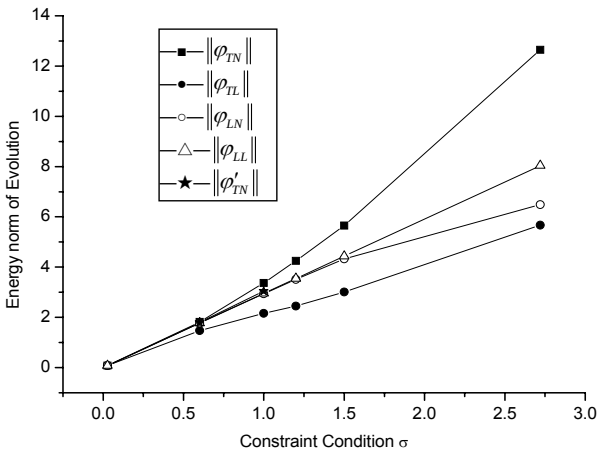

Fig. 1. Linear and nonlinear numerical results of CNOP and LSV for an integration time of 10 days for Expt. 1.

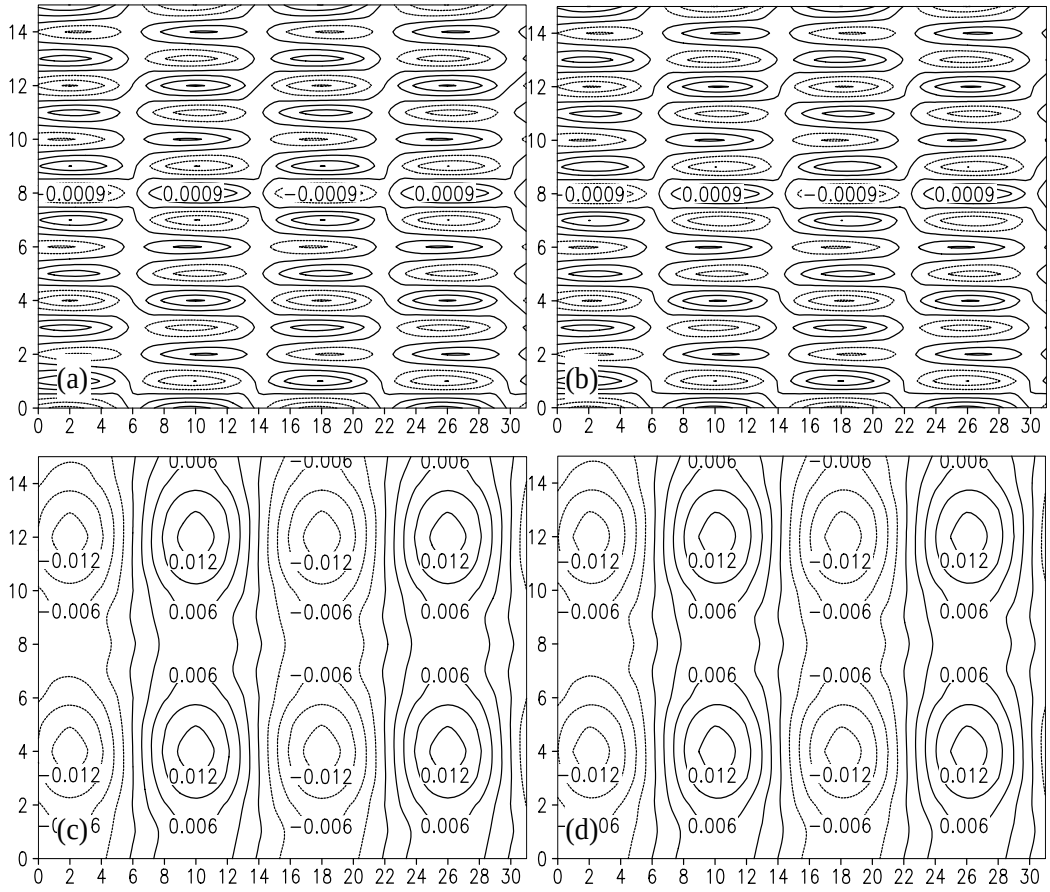

Fig. 2. Results of the small constraint condition for an integration time of 10 days for Expt. 1, in which the x-axis represents the zonal direction, the y-axis represents the meridional direction, and the value is dimensionless length (Fig. 3, Fig. 6 and Fig. 7 are the same as Fig. 2) (a) LSV with $\sigma = 0.0272$ [Contour interval (CI) is 3.0×10^{-4}]; (b) CNOP with σ=0.0272 (CI=3.0×10^{-4}); (c) Linear evolution of SV (CI=0.003); (d) Nonlinear evolution of CNOP(CI=0.003).

sults show that the patterns of LSV and its linear evolution are the same as Figs. 2a and c respectively, where the only differences between them are the values. The patterns of CNOPs and LSVs are compared, and we find that regardless of the local CNOP or global CNOP, they show differences from LSV. Certainly, the local CNOP shows more similarity to the LSV than the global CNOP. That is to say, under such a condition, the linear approximation is invalid and CNOP may describe the phenomena exactly.

3.2 *Experiment 2*

In this experiment, another zonal basic state is chosen, where $a = 4.478$ and $b = 42.685$. This is also a steady state. According to Arnol'd's nonlinear stability criteria, this basic state is more stable than the first one. The energy norm of the basic state is 259.78. The maximum constraint condition σ of the initial perturbation is 5.2, which is approximately 2.0% of that of the basic state.

Table 2 summarizes the numerical results of Experiment 2. Figure 4, like Fig. 2, gives the evolution of CNOPs and LSVs with different initial constraint conditions. Under the very small initial constraint condition, the linear approximation is valid. The value of λ_{L} can represent the degree of stability. The smaller the value is, the more stable the basic state is. Under the large initial constraint condition, we can compare the CNOP in Expt.2 whose ratio to the basic state is the same as that in Expt. 1. The smaller the energy norm of their corresponding nonlinear evolutions to the basic state is, the more stable the basic state is. The numerical results prove that this basic state is certainly more stable than the first one. Considering the similarity of the basic state between Expt. 1 and Expt. 2, the patterns of LSVs and CNOPs are omitted.

Table 1. Nonlinear and linear numerical results of CNOP and LSV for an integration time of 10 days for Expt. 1.

σ	$\| \varphi_{\rm TN} \|$	$\| \varphi_{\rm TL} \|$	$\| \varphi_{\rm LN} \|$	$\| \varphi_{\rm LL} \|$	$\lambda_{\rm L}$
2.72×10^{-2}	8.043×10^{-2}	8.042×10^{-2}	8.042×10^{-2}	8.042×10^{-2}	2.957
0.60	1.798	1.730	1.774	1.773	–
	1.819	1.472			
1.0	3.042	2.884	2.941	2.957	–
	3.371	2.160			
1.2	4.253	2.452	3.511	3.548	–
1.5	5.653	3.013	4.327	4.435	–
2.72	12.652	5.669	6.488	8.042	–

Table 2. Nonlinear and linear numerical results of CNOP and LSV for an integration time of 10 days for Expt. 2.

σ	$\| \varphi_{\rm TN} \|$	$\| \varphi_{\rm TL} \|$	$\| \varphi_{\rm LN} \|$	$\| \varphi_{\rm LL} \|$	$\lambda_{\rm L}$
2.6×10^{-2}	7.483×10^{-2}	7.482×10^{-2}	7.482×10^{-2}	7.482×10^{-2}	2.878
0.6	1.752	1.703	1.725	1.727	–
1.0	2.973	2.785	2.860	2.878	–
2.6	10.471	4.517	6.079	7.482	–
	11.248	5.083			
5.2	20.742	9.328	7.541	14.965	–
	22.180	10.570			

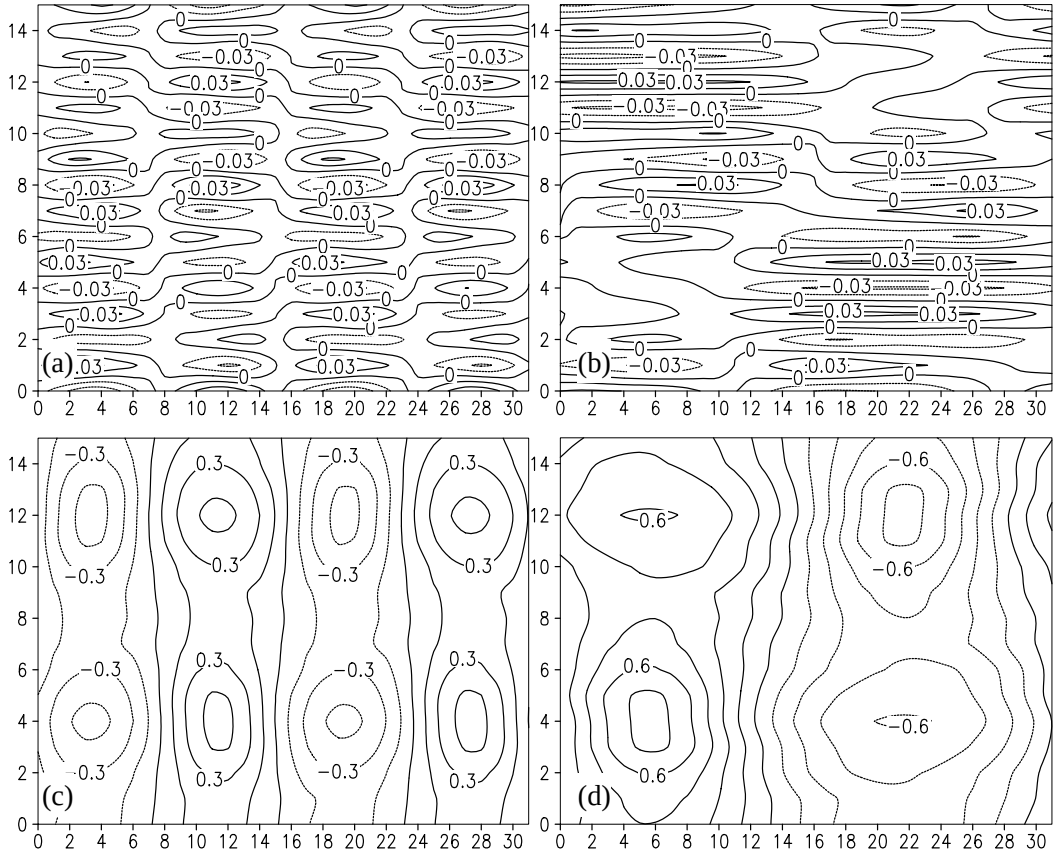

Fig. 3. Results of large constraint condition for an integration time of 10 days for Expt. 1. (a) Local CNOP with $\sigma = 1.0$ (CI=0.015); (b) Global CNOP with $\sigma = 1.0$ (CI=0.015); (c) (CI=0.1) and (d) (CI=0.2) correspond to the nonlinear evolution of (a) and (b) respectively.

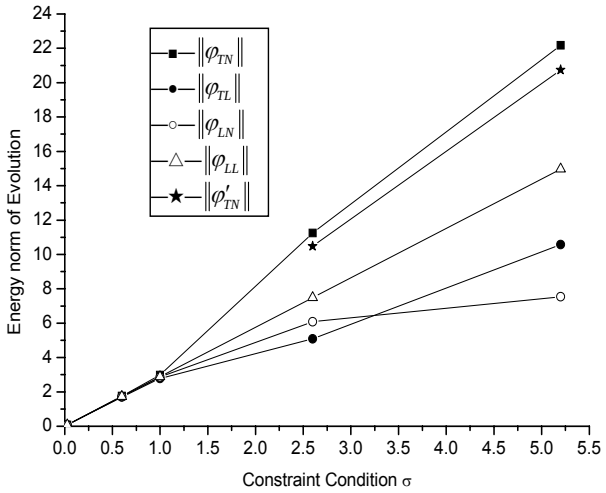

Fig. 4. Nonlinear and linear numerical results of CNOP and LSV for an integration time of 10 days for Expt. 2.

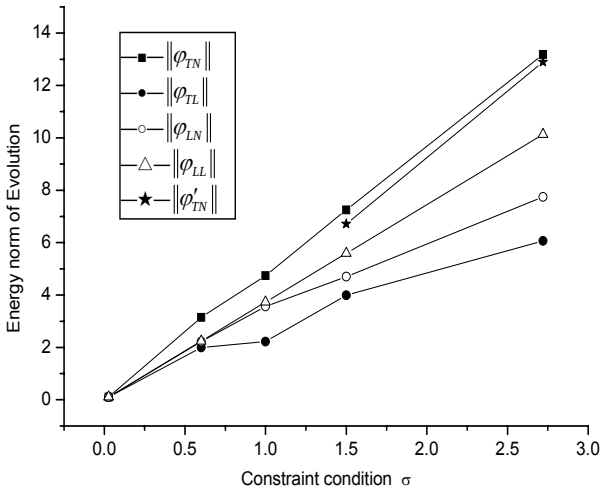

Fig. 5. Nonlinear and linear numerical results of CNOP and LSV for an integration time of 10 days for Expt. 3.

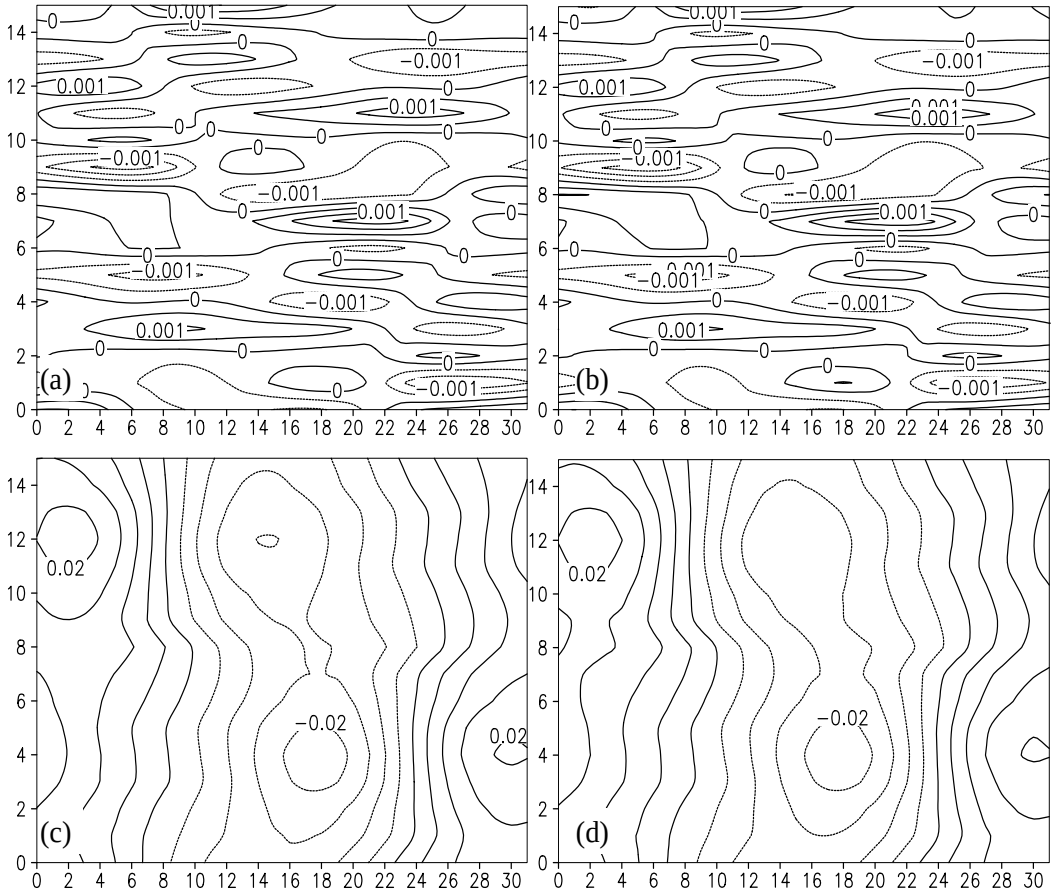

Fig. 6. Results of the small constraint condition for an integration time of 10 days for Expt. 3. (a) LSV with $\sigma = 0.0272$ (CI=5.0×10^{-4}); (b) CNOP with $\sigma = 0.0272$ (CI=5.0×10^{-4}); (c) Linear evolution of SV (CI=0.005); (d) Nonlinear evolution of CNOP (CI=0.005).

Table 3. Nonlinear and linear numerical results of CNOP and LSV for an integration time of 10 days for Expt. 3.

σ	$\parallel \varphi_{\rm TN} \parallel$	$\parallel \varphi_{\rm TL} \parallel$	$\parallel \varphi_{\rm LN} \parallel$	$\parallel \varphi_{\rm LL} \parallel$	$\lambda_{\rm L}$
2.72×10^{-2}	0.102	0.101	0.101	0.101	3.725
0.60	3.152	2.000	2.217	2.235	–
1.0	4.736	2.218	3.556	3.725	–
1.5	6.712	3.824	4.703	5.587	–
	7.247	3.991			
2.72	12.895	5.945	7.744	10.132	–
	13.188	6.071			

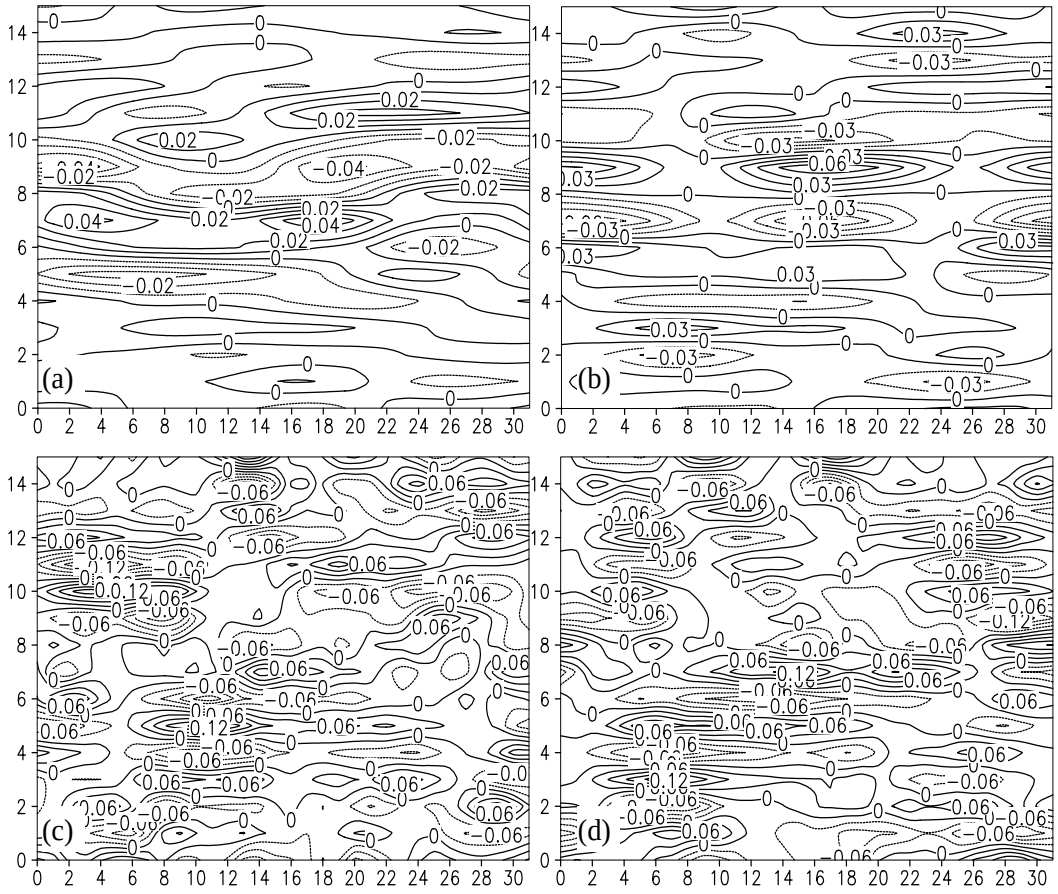

Fig. 7. Results of the large constraint condition for an integration time of 10 days for Expt. 3. (a) CNOP with the energy norm of 0.6 (CI=0.01). (b) CNOP with the energy norm of 1.0 (CI=0.015); (c) Local CNOP with the energy norm of 2.72 (CI=0.03); (d) Global CNOP with the energy norm of 2.72 (CI=0.03):

3.3 *Experiment 3*

In the last experiment, an unsteady basic state is given. The basic state is obtained by integrating the following initial field,

$$\psi_0(x,y) = a \times \sin\left(\frac{2\pi y}{2Y}\right) + b \times \sin\left(\frac{2\pi y}{2Y}\right) + c\,,$$

where $a = 0.5$, $b = 4.62$ and $c = 44.643$. This non-zonal initial field is obtained by adding a weak meridional flow on the basis of Expt. 1. So this basic state perhaps is an unstable flow according to Arnol'd's stability criteria. The energy norm of the initial basic state is 271.643. The maximum constraint condition σ of the initial perturbation is 2.72, which is approximately 1.0% of that of the basic state.

Table 3 summarizes the numerical results of Ex-

periment 3. Figure 5, like Fig. 2, gives the evolution of CNOPs and LSVs with different initial constraint conditions. The numerical results prove that this basic state is certainly less stable than the first one. Figure 6 gives the LSV and CNOP with energy norm 0.0272 for 10 days and their corresponding linear and nonlinear evolutions. Similar to the above two experiments, the patterns of CNOP and LSV and their corresponding nonlinear and linear evolutions are very similar under the condition that the initial constraint condition is very small. Figure 7 shows CNOPs with different initial constraint conditions. With the initial constraint condition σ increasing, the CNOPs show great differences from the LSV gradually, which is due to the fact that the CNOPs have begun to display the nonlinear characteristics of the system. Besides, the results do not show the difference of the scale between the local CNOP and global CNOP, which, in Mu and Zhang (2006), the scale of the global CNOP is usually smaller than that of the local CNOP. For a complex model with large free degrees, the relationship between the local and global CNOP needs to be explored further.

4. Conclusions and implications

In this paper, the conditional nonlinear optimal perturbation and singular vector are both obtained numerically with a two-layer quasi-geostrophic model in a small-scale vortex in Jupiter's atmosphere. Under the condition that the initial constraint condition is very small, LSV and CNOP are very similar for not too long optimization time interval, and the linear approximation is valid. With the initial constraint condition increasing, CNOP and LSV show great differences regardless of their patterns or their evolutions. In this case, the linear approximation is invalid and CNOP can catch the nonlinear characteristics better. Furthermore, for some basic states, local CNOPs can be obtained except for the global CNOPs.

Because, in this paper, the lower and upper flows are both simplified, this may not represent the real status of Jupiter's atmosphere. But the application of the CNOP method to the theoretical model of motion in a small-scale vortex in Jupiter's atmosphere may provide the chance for us to continue to compare the stability of motions of Jupiter's atmosphere and the Earth's atmosphere. Thus we can further understand the motion of Earth's atmosphere.

Besides, the problem of stability of flows around a large-scale vortex, such as the GRS, in Jupiter's atmosphere is also intriguing. It is known that the reduced-gravity shallow water model can simulate this phenomenon well (Dowling and Ingersoll, 1989). So, encouraged by the numerical results above, the method of CNOP can be applied to the reduced-gravity shallow water model to study the stability of flows around a large-scale vortex.

Acknowledgments. The work was jointly supported by the Chinese Academy of Sciences (Grant No. KZCX3-SW-230) and the National Natural Science Foundation of China (Grant Nos. 40233029 and 40221503). This work was finished under the guidance of Prof. Mu Mu, and great thanks are given to Prof. Zhiyue Zhang for his help in drawing the figures.

REFERENCES

Achterberg, R. K., and A. P. Ingersoll, 1994: Numerical simulation of baroclinic Jovian vortices. *J. Atmos. Sci.*, **51**, 541–562.

Birgin, E. G., J. M. Martinez, and M. Raydan, 2000: Nonmonotone spectral projected gradient methods on convex sets. *SIAM Journal of Opt.*, **10**(4), 1196–1211.

Dowling, T. E., 1993: A relationship between potential vorticity and zonal wind on Jupiter. *J. Atmos. Sci.*, **50**, 14–22.

Dowling, T. E., and A. P. Ingersoll, 1988: Potential vorticity and layer thickness variations in the flow around Jupiter's Great Red Spot and White Oval BC. *J. Atmos. Sci.*, **45**, 1380–1396.

Dowling, T. E., and A. P. Ingersoll, 1989: Jupiter' Great Red Spot as a shallow water system. *J. Atmos. Sci.*, **46**(21), 3256–3278.

Duan, W. S., M. Mu and B. Wang, 2004: Conditional nonlinear optimal perturbations as the optimal precursors for ENSO events. *J. Geophys. Res.*, **109**, D23105, doi:10.1029/2004JD004756.

Gill, A. E., 1982: *Atmosphere-Ocean Dynamics*. Academic Press, New York, 662pp.

Ingersoll, A. P., 1990: Atmospheric dynamics of the outer planets. *Science*, **248**, 308–315.

Ingersoll, A. P., and P. G. Cuong, 1981: Numerical model of long-lived Jovian vortices. *J. Atmos. Sci.*, **38**, 2067–2076.

Lorenz, EN, 1965: A study of the predictability of a 28-variable model. *Tellus*, **17**, 321–333.

MacLow, M. M., and A. P. Ingersoll, 1986: Merging of vortices in the atmosphere of Jupiter: An analysis of Voyager images. *Icarus*, **65**, 353–369.

Marcus, P. S., 1988: Numerical simulation of Jupiter's Great Red Spot. *Nature*, **331**, 693–696.

Mu, M., and T. G. Shepherd, 1994: On Arnol'd's second nonlinear stability theorem for two-dimensional quasi-geostrophic flow. *Geophys. Astrophys. Fluid Dyn.*, **75**, 21–37.

Mu Mu, and Duan Wansuo, 2003: A new approach to studying ENSO predictability: Conditional nonlinear optimal perturbation. *Chinese Science Bulletin*, **48**, 747–749.

Mu, M., and Z. Y. Zhang, 2006: Conditional nonlinear optimal perturbations of a two-dimensional quasi-geostrophic model. *J. Atmos. Sci.*, **63**(6), 1587–1604.

Mu, M., W. S. Duan, and B. Wang, 2003: Conditional nonlinear optimal perturbation and its application. *Nonlinear Processes in Geophysics*, **10**, 493–501.

Mu, M., L. Sun, and H. A. Dijkstra, 2004: The sensitivity and stability of the ocean's thermohaline circulation to finite amplitude perturbations. *Journal of Physical Oceanography*, **34**, 2305–2315.

Powell, M. J. D., 1982: VMCWD: A FORTRAN subroutine for constrained optimization, DAMTP Report 1982/NA4, England, University of Cambridge, 1–89.

Williams, G. P., 1996: Jovian dynamics. Part 1: Vortex stability, structure, and genesis. *J. Atmos. Sci.*, **53**, 2685–2734.

Williams, G. P., and T. Yamagata, 1984: Geostrophic regimes, intermediate solitary vortices and Jovian eddies. *J. Atmos. Sci.*, **41**(4), 453–478.